Onsager's reciprocal relation and the hydraulic permeability of porous media

Sidney X. Li, David B. Pengra, and Po-zen Wong*
Department of Physics and Astronomy, University of Massachusetts, Amherst, Massachusetts 01003-3720
(Received 23 May 1994)

The coupling between fluid and electric currents in random porous media leads to two reciprocal electrokinetic phenomena known as streaming potential and electro-osmosis. We report an experimental study of these coupling coefficients in rock and sintered glass bead samples. Using Onsager's reciprocal relation, we show that they rigorously determine the effective pore size for transport and hydraulic permeability of porous media.

PACS number(s): 47.55.Mh, 61.43.−j, 82.65.Fr

The flow of fluid in rigid porous media is known to obey Darcy's law [1]

$$\mathbf{J}_f = -\frac{k_D}{\eta}\nabla P \ , \tag{1}$$

which is an analog of Ohm's law for electrical conduction. Here, $\mathbf{J}_f$ is the fluid volume current density which has the unit of velocity, P is the viscous pressure field that drives the flow, η is the fluid viscosity, and k_D is the hydraulic permeability of the porous media. $\mathbf{J}_f$ is also known as the Darcy velocity and k_D the Darcy permeability. There has been much interest in understanding how the microscopic structure of the porous media affects the value of k_D because it is one of the most important parameters that determine how fast oil and gas can be produced from reservoir rocks [2]. In this paper, we show how electrokinetic phenomena due to the coupling between the fluid and electric currents can be used to determine k_D and the relevant pore radius for transport.

For brine saturated rock, one expects k_D to be related to the electrical conductivity (σ_r), because both the fluid and the charge move through the same pore space. The main parameter that governs such transport phenomena is called the formation factor F, defined as the ratio σ_w/σ_r, where σ_w is the brine conductivity. Since the rock matrix is insulating, $F>1$ always holds. Using artificial rock samples made of fused glass beads (FGB), Wong, Koplik, and Tomanic (WKT) showed that $k_D \approx D_b^2/78F^2$, where D_b is the bead diameter [3]. In contrast, Katz and Thompson (KT) studied a suite of rock and found that $k_D \approx l_c^2/226F$, where l_c is a characteristic hydraulic pore diameter obtained by mercury injection [4]. These two results can be reconciled by considering the rock as made up of statistically equivalent building blocks of size ξ_b^3, each of which is penetrated by a cylindrical tube of radius $R_{\rm eff}$ [2]. This model predicts $F=\xi_b^2/\pi R_{\rm eff}^2$, and

$$k_D = \pi R_{\rm eff}^4/8\xi_b^2 = \xi_b^2/8\pi F^2 = R_{\rm eff}^2/8F \ . \tag{2}$$

Since $\xi_b \propto D_b$ and $l_c \propto R_{\rm eff}$, the results of WKT and KT are consistent. Theoretically, Johnson, Koplik, and Schwartz [5] proposed an analog of Eq. (2):

$$k_D \approx \Lambda^2/8F \ , \tag{3}$$

where Λ is a pore radius defined by the solution of Laplace's equation in the pore space. For fully connected pores, Λ, l_c, and $R_{\rm eff}$ all have the same qualitative meaning and so do Eqs. (2) and (3). These results prompted much interest in studying how the pore size affects other properties of porous media [6]. The hope is to find the pore size by other measurements and use it to deduce the permeability. In the following, we describe how the studies of electrokinetic phenomena achieve this purpose and provide some new understanding of transport in porous media.

At a brine-solid interface, a thin layer of ionic space charge exists on the liquid side due to the difference in electron energy levels across the interface, much like a p-n junction between semiconductors. This is known as the Debye-Hückle layer or the Guoy-Chapman layer [7]. Its thickness (δ) is about 1 nm for 0.1 M NaCl brine. When the fluid flows it drags the ions in the layer along, thereby forming an electric current. Conversely, under an applied electric field ($-\nabla\Phi$), the migration of the interfacial charge drags the neutral fluid. Formally, the coupled flow of charge and fluid currents are described by two linear equations:

$$\mathbf{J}_e = -\sigma_0\nabla\Phi - L_{12}\nabla P \ , \tag{4a}$$

$$\mathbf{J}_f = -L_{21}\nabla\Phi - \frac{k_0}{\eta}\nabla P \ , \tag{4b}$$

where $\mathbf{J}_e$ is the electric current density. The diagonal terms are the usual Ohm's law and Darcy's law for uncoupled flow. The off-diagonal terms represent the coupling due to the interfacial charge. Because $-\mathbf{J}_e\cdot\nabla\Phi$ and $-\mathbf{J}_f\cdot\nabla P$ correspond to the rate of heat production per unit volume, the off-diagonal coefficients must satisfy the Onsager's reciprocal relation in the steady state: $L_{12}=L_{21}\equiv\Pi$ [8]. Streaming potential (STP) arises when

*Electronic address: PZWONG@PHAST.UMASS.EDU

there is only an applied pressure driving the fluid flow. Setting $\mathbf{J}_e=0$ in Eq. (4a) shows that an applied pressure difference ΔP_a between any two points leads to a potential difference $\Delta\Phi_S=-K_S\Delta P_a$, where $K_S=\Pi/\sigma_0$. Similarly, electro-osmosis (ELO) occurs when only an applied potential difference $\Delta\Phi_a$ drives an electric current so that $\mathbf{J}_f=0$ in Eq. (4b). This results in a pressure difference $\Delta P_e=-K_E\Delta\Phi_a$, where $K_E=\Pi\eta/k_0$. Eliminating Π between K_S and K_E gives $k_0=\eta\sigma_0K_S/K_E$. Thus measuring σ_0, K_S and K_E rigorously determines k_0. However, σ_0 and k_0 are not the same as σ_r and k_D obtained in typical experiments, because σ_r is the apparent conductivity when $\mathbf{J}_f=0$ and k_D is the apparent permeability when $\mathbf{J}_e=0$. From Eq. (4) and the definition of K_S and K_E, one can show that $\sigma_r=\sigma_0(1-K_SK_E)$ and $k_D=k_0(1-K_SK_E)$. Hence

$$k_D=\eta\sigma_rK_S/K_E \tag{5}$$

must hold in the dc limit.

The simplest realization of Eq. (5) is in a cylindrical capillary tube with a radius R_{eff} much larger than δ. From the fluid velocity field in the tube and the charge density profile at the wall one finds that $\Pi=\varepsilon_w\zeta/\eta$, where ε_w is the dielectric permittivity of brine and ζ is the potential at the slip plane of the brine [7]. It follows that $K_S=\varepsilon_w\zeta/\eta\sigma_w$, $K_E=8\varepsilon_w\zeta/R_{\text{eff}}^2$, or equivalently

$$R_{\text{eff}}^2=8\eta\sigma_wK_S/K_E, \tag{6a}$$

and

$$\zeta=K_S\eta\sigma_w/\varepsilon_w\ . \tag{6b}$$

Clearly, using Eq. (6a) in Eq. (2) satisfies Eq. (5), so it may be regarded as the working definition of an *effective pore radius* in random porous media. Likewise, Eq. (6b) defines an *effective ζ potential* for irregular pore surfaces.

We tested the above predictions in a suite of real and artificial rock which consists of six sandstones, two limestones, and four FGB samples. Because the STP and ELO signals are typically much less than the interfacial voltage noise associated with the probing electrodes, we perform all measurements at finite frequency using a digital lock-in technique to overcome the signal-to-noise problem. This technique is capable of covering a frequency range from 10^5 Hz down to 10^{-4} Hz, so that we can estimate the dc values from the low frequency data. Two sets of instruments are used: a Solartron 1286 Electrochemical Interface and 1254 Frequency Response Analyzer are used to measure the ac conductivity (σ_r) and the ac electro-osmosis (K_E); an HP-3562A dynamic signal analyzer and a pair of high impedance preamplifiers are used to measure the ac streaming potential (K_S). The samples are cylindrical in shape, about 1.9 cm in diameter and 3.8 cm in length. They are vacuum impregnated with 0.1 M NaCl brine so that no air is trapped inside the pores. They are mounted in an acrylic cell with two end cavities filled with the same brine and connected only through the porous sample. Care was taken to remove all trapped air in the cavities. Ring electrodes around the two ends of the samples are used to probe the voltage across it. Disk electrodes placed 2 cm from the two end faces of the sample are used to inject current. All the electrodes are made of thin solid silver plates with a Ag/AgCl surface. The pressure drop across the sample is detected by an Omega PX160 piezoresistive transducer which has a sensitivity of 10 mV/psi, or about 1.5 μV/Pa (1Pa$\equiv$1N/m^2). For STP measurements, an ac applied pressure is generated by a push rod attached to a loudspeaker driven by a power amplifier. Through a Latex membrane, it pushes on the fluid in one end of the cell and creates oscillation amplitudes up to 5 kPa (about 0.5 psi) at low frequencies.

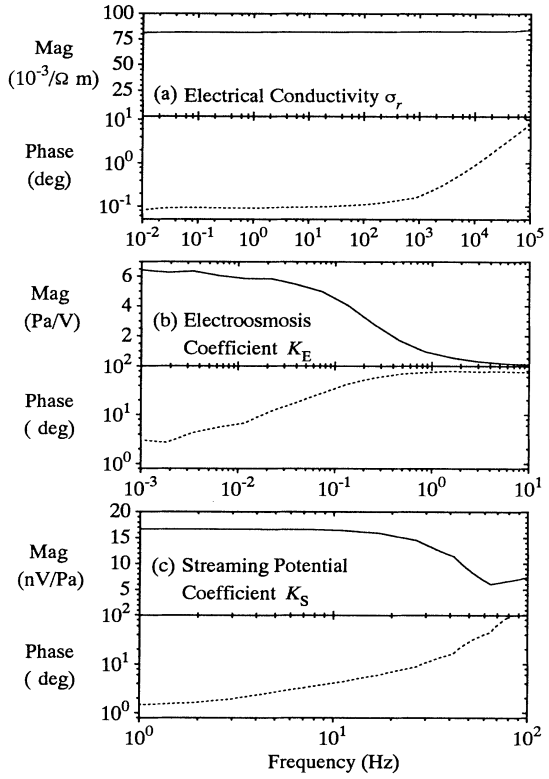

FIG. 1. The complex (magnitude and phase) frequency response of a Berea sandstone illustrates the typical behavior seen among the 12 samples. (a) Electrical conductivity σ_r; (b) electro-osmosis coefficient K_E; (c) streaming potential K_S.

Figures 1(a)–1(c) show the complex frequency response of σ_r, K_E, and K_S, respectively, for a Berea sandstone. We observe that σ_r is essentially constant below 1 kHz. The slight dispersion above 1 kHz is due to the stray capacitance in the measurement circuit. On close examination, however, one can see that the magnitude decreases towards lower frequency at about 1% per decade. A small phase angle about 0.1° persists down to 10 mHz. This behavior is known to exist in sandstone and believed to be caused by the cations on the clay surface [9]. We also observe similar small phase angles for K_E and K_S at low frequencies. These observations support the notion that the effects are caused by the interfacial charge, but the detailed mechanism is not understood. This is a topic

TABLE I. Summary of the measured and calculated properties of 12 samples saturated with 0.1 M NaCl brine. The rock conductivity σ_r and the two electrokinetic coefficients K_S and K_E are measured by our ac technique. These are used to calculate the electrokinetic permeability k_e, and ζ potential, and the effective pore radius R_{eff} according to Eqs. (5) and (6). The Darcy permeability k_D is measured by the standard dc flow method. The errors for K_S, K_E, and k_D are discussed in the text. The errors for F are mainly due to the inaccuracies in the sample dimensions and they do not affect the comparison between k_e and k_D.

Sample	Porosity ϕ (%)	F (σ_w/σ_r)	K_S (nV/Pa)	K_E (Pa/V)	k_e (mdarcy)	k_D (mdarcy)	ζ (mV)	R_{eff} (μ_m)
				Sandstones				
Fontainebleau *A*	22.3	12.1(1.2)	13.8(2.1)	0.623(0.068)	1760(440)	1530(260)	18.4(3.7)	12.9(1.5)
Fontainebleau *B*	16.8	21.7(2.2)	19.8(1.8)	0.737(0.13)	1190(310)	852(150)	26.5(4.3)	14.3(1.7)
Fontainebleau *C*	6.70	160(16)	14.8(1.6)	30.2(3.9)	2.93(0.70)	4.72(1.1)	19.7(3.4)	1.93(0.21)
Berea *A*	22.9	11.9(2.0)	16.4(2.0)	6.15(1.4)	215(73)	323(57)	21.9(4.0)	4.50(0.66)
Berea *B*	20.5	20.6(2.1)	15.0(1.1)	37.2(0.98)	18.7(3.5)	23.9(4.2)	20.0(3.1)	1.75(0.14)
Bandera	21.9	12.9(1.8)	10.9(0.44)	728(27)	1.11(0.22)	0.822(0.14)	14.5(2.1)	0.336(0.03)
				Limestones				
Whitestone	26.0	20.3(2.0)	5.94(1.2)	32.3(6.7)	8.71(2.9)	6.69(1.3)	7.94(1.9)	1.18(0.19)
Indiana	15.0	35.9(3.6)	10.9(0.36)	35.5(4.2)	8.16(1.7)	4.55(0.77)	14.5(2.0)	1.52(0.14)
				Fused glass beads				
50 μm *A*	10.1	56.0(5.6)	13.0(1.4)	49.4(6.5)	4.51(1.1)	6.05(1.0)	17.4(3.0)	1.41(0.15)
50 μm *B*	17.1	16.0(1.6)	18.6(0.71)	12.5(1.7)	89.1(20)	66.5(11)	24.8(3.5)	3.36(0.33)
100 μm	19.3	12.2(1.2)	15.1(1.3)	1.90(0.36)	622(170)	540(95)	20.1(3.3)	7.75(0.96)
200 μm	29.8	10.3(1.0)	14.2(2.6)	0.252(0.033)	5230(1500)	4600(780)	18.9(4.3)	20.6(2.7)

under study. For the purpose of estimating the dc values needed in Eqs. (5) and (6), we shall regard this as a source of small systematic error.

The frequency response of K_E and K_S show additional relaxations below 100 Hz. That of K_S in Fig. 1(c) was found to be due to the mechanical behavior of the PX160 transducer. Replacing it with a piezoelectric transducer with a fast mechanical response yielded an essentially constant value below 100 Hz. This behavior is expected because dc flow should occur below a viscous relaxation frequency given by $f_c=\eta/\pi R_{\text{eff}}^2\rho$, where ρ is the fluid density [10]. With water at room temperature and a tube radius $R_{\text{eff}}=20$ μm, one finds $f_c\approx 1$ kHz. This is a lower bound of the relaxation frequency f_S for the STP signal because STP only senses the fluid flow in the charge layer with thickness $\delta\approx 1$ nm. Estimating f_S by $f_c(R_{\text{eff}}/\delta)^2$ puts it far above our measurement range. The relaxation of K_E in Fig. 1(b) was found to be related to our cell design. It comes from the fact that a small volume of fluids has to be moved across the sample to create compression and decompression on the fluid in the end cavities, and that requires a finite amount of time τ. The relaxation frequency is just given by $f_E=1/2\pi\tau$. In our cell, the cavities are cylindrical and have the same radius as the sample. This relaxation can be modeled as a one dimensional problem and solved analytically. The predictions of the model were verified by changing various cell parameters. These details will be described elsewhere. What we emphasize here is merely that the ac technique has high enough sensitivity to determine the very small coupling constants K_E and K_S. In addition, having accounted for the various causes for dispersion lend confidence that we can use the low frequency data to approximate the true dc values that enter Eqs. (5) and (6).

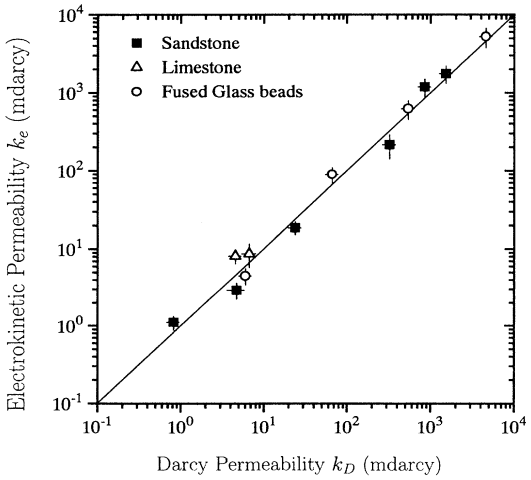

FIG. 2. A comparison between the electrokinetic permeability k_e and the Darcy permeability k_D confirms the prediction of Eq. (5).

Table I tabulates the results for the 12 samples. F, K_S, and K_E are the measured quantities at sufficiently low frequencies. We note that $K_EK_S \ll 10^{-6}$ holds for all the samples. Thus the distinction between (σ_0,k_0) and (σ_r,k_D) can be ignored. k_e is the electrokinetic permeability determined by the right-hand side of Eq. (5): $k_e\equiv\eta\sigma_rK_S/K_E$. k_D is the dc Darcy permeability which we measured separately by injecting a constant fluid current through the sample and monitoring the pressure drop across it. Figure 2 shows the comparison between

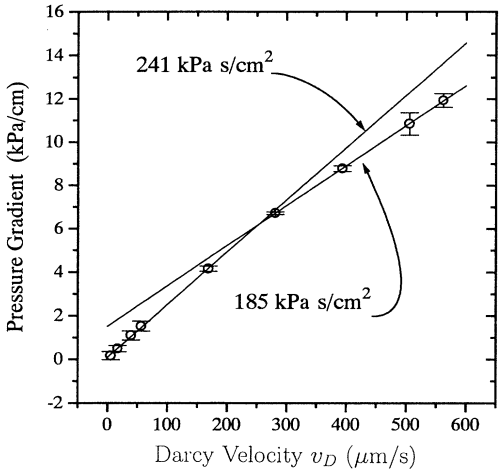

FIG. 3. The nonlinear relationship between the Darcy velocity and the pressure gradient in Berea sandstone is typical of all the samples. The slope of the curve gives η/k_D. The data show that the apparent k_D increases at higher pore fluid pressure.

k_e and k_D. Evidently Eq. (5) successfully predicts the permeability over a range of about four decades with no adjustable parameters. The error bars we assigned to k_e reflect our *estimates* for the difference between the low frequency data and the true dc values. They are obtained from the variation of the data over the lowest decade of frequency measured. The error bars for k_D have a different origin. In Fig. 3, we show how the pressure across a Berea sandstone increases with the Darcy velocity (v_D). The data are manifestly nonlinear. The reason is that rock and FGB are not as rigid as they appear. Their elastic properties are dominated by the small contact areas between neighboring grains [11]. When the pore fluid is pressurized, sheetlike pores expand and enhance the permeability. The values of k_D listed in Table I are obtained with ΔP_a below 10 kPa and the error bars account for variations up to about 50 kPa. Despite these systematic errors, the agreement between k_D and k_e shows the validity of Eq. (5) and the power of Onsager's relation.

The last two columns of Table I give the values of ζ and R_{eff} calculated from Eqs. (6a) and (6b). We note that the concept of the ζ potential is traditionally defined for a flat surface only. Since the pore surfaces in sandstone are known to have fractal roughness [2], the *effective* values of ζ we obtained are sensitive to the charge layer thickness δ, which varies with brine concentration. This is a topic under investigation. The values of R_{eff} as explained above, represent *effective pore radii* for the different samples that rigorously obey Eq. (2). Until now, this conceptual parameter has eluded precise theoretical definition and experimental determination. We believe these microscopic parameters will help us to understand other macroscopic properties of porous media.

This work was supported by the Gas Research Institute Contract No. 5090-260-1953. We have also benefited from National Science Foundation Grant Nos. DMR-8922830 and DMR-9404672.

[1] See, e.g., F. A. L. Dullien, *Porous Media: Fluid Transport and Pore Structure* (Academic, San Diego, 1979).

[2] For recent reviews, see, e.g., P.-z. Wong, MRS Bull. **19**, 32 (1994); Phys. Today **41** (12), 24 (1988).

[3] P.-z. Wong, J. Koplik, and J. P. Tomanic, Phys. Rev. B **30**, 6606 (1984).

[4] A. J. Katz and A. H. Thompson, Phys. Rev. B **34**, 8179 (1986).

[5] D. L. Johnson, J. Koplik, and L. M. Schwartz, Phys. Rev. Lett. **57**, 2564 (1986).

[6] See, e.g., J. Koplik, C. Lin, and M. Vermette, J. Appl. Phys. **56**, 3127 (1984); J. G. Berryman and S. C. Blair, *ibid.* **60**, 1930 (1986); J. R. Banavar and L. M. Schwartz, Phys. Rev. Lett. **58**, 1411 (1987); P. P. Mitra, P. N. Sen, L. M. Schwartz, and P. Le Doussal, *ibid.* **68**, 3555 (1992); R. L. Kleinberg, Magn. Reson. Imag. **12**, 271 (1994), and references therein.

[7] See, e.g., G. Kortüm, *Treatise on Electrochemistry,* 2nd ed. (Elsevier, Amsterdam, 1965).

[8] See, e.g., S. R. de Groot and P. Mazur, *Nonequilibrium Thermodynamics* (Dover, Mineola, 1984).

[9] H. J. Vinegar and M. H. Waxman, Geophysics **49**, 1267 (1984).

[10] D. L. Johnson, J. Koplik, and R. Dashen, J. Fluid Mech. **176**, 379 (1987).

[11] See, e.g., M. H. Cohen, in *Physics and Chemistry of Porous Media II,* edited by J. R. Banavar, J. Koplik, and K. Winkler, AIP Conf. Proc. No. 154 (AIP, New York 1987).